


Article

Effects of C-Terminal Carboxylation on α -Conotoxin LsIA Interactions with Human α 7 Nicotinic Acetylcholine Receptor: Molecular Simulation Studies

Jierong Wen *  and Andrew Hung *

School of Science, College of Science, Engineering and Health, RMIT University, Melbourne, VIC 3001, Australia

* Correspondence: s3497075@student.rmit.edu.au (J.W.); Andrew.Hung@rmit.edu.au (A.H.)

Received: 4 March 2019; Accepted: 27 March 2019; Published: 2 April 2019



Abstract: α -Conotoxins selectively bind to nicotinic acetylcholine receptors (nAChRs), which are therapeutic targets due to their important role in signaling transmission in excitable cells. A previous experimental study has demonstrated that carboxylation of the C-terminal of α -conotoxin LsIA reduces its potency to inhibit human α 7 nAChR relative to naturally amidated LsIA. However, little is known about the contribution of conformational changes in the receptor and interactions, induced by C-terminal amidation/carboxylation of conotoxins, to selective binding to nAChRs, since most conotoxins and some disulfide-rich peptides from other conotoxin subfamilies possess a naturally amidated C-terminal. In this study, we employ homology modeling and molecular dynamics (MD) simulations to propose the determinants for differential interactions between amidated and carboxylated LsIAs with α 7 nAChR. Our findings indicate an overall increased number of contacts favored by binding of amidated LsIA versus its carboxylated counterpart. Toxin-receptor pairwise interactions, which may play a role in enhancing the potency of the former, include ARG10-TRP77, LEU141 and CYS17-GLN79 via persistent hydrogen bonds and cation- π interactions, which are weakened in the carboxylated form due to a strong intramolecular salt-bridge formed by ARG10 and carboxylated C-terminus. The binding of amidated LsIA also induces enhanced movements in loop C and the juxtamembrane Cys-loop that are closely associated with receptor function. Additionally, the impacts of binding of LsIA on the overall structure and inter-subunit contacts were examined using inter-residue network analysis, suggesting a clockwise tilting of the α 7 C and F loops upon binding to carboxylated LsIA, which is absent for amidated LsIA binding. The predicted molecular mechanism of LsIA binding to the α 7 receptor may provide new insights into the important role of the C-terminal in the binding potency of conotoxins at neuronal nAChRs for pharmacological purposes.

Keywords: homology modeling; MD simulation; α -conotoxin; nicotinic acetylcholine receptor; C-terminal amidation/carboxylation

1. Introduction

nAChRs are situated in the plasma membranes of certain neurons in the central and peripheral nervous systems [1]. These ligand-gated ion channels are involved in signal transmission, neuronal integration and cell excitability through activation by acetylcholine (ACh) binding [1]. There are two general types of nAChRs, heteropentamers and homopentamers, both forming a cylindrical helical bundle around the ion pore [2]. The homomeric nAChRs are constituted by 5 identical subunits, whereas heteropentameric nAChRs consist of distinct subunits which may include combinations of α 1-10, β 1-4, γ , δ and ϵ subunits [3]. The various combinations of subunits also render distinct nAChRs with unique physiological and pharmacological properties [4].

Human $\alpha 7$ nAChR subtype, as an example of homopentameric nAChRs, has been extensively studied due to its important function in cognitive processes and an implicated involvement in the cholinergic anti-inflammatory pathway [5]. The dysfunction of $\alpha 7$ nAChR, therefore, is related to many neurological diseases and disorders, such as schizophrenia [6,7], Alzheimer's disease and Parkinson's disease [1,8–10]. The determination of the crystal structures of acetylcholine binding protein (AChBP) complex to conotoxins has enabled the construction of molecular models of human $\alpha 7$ nAChR bound to conotoxins [6,11,12], although detailed structural information on toxin-bound nAChRs is currently relatively scarce. Even if the similarities between sequences of AChBP [13] and the extracellular domain (ECD) (the region for acetylcholine (ACh) binding [14]) of human $\alpha 7$ receptor are less than 30% [15,16], up to 52% of its sequence at the ligand binding domain (LBD) is identical to the ligand binding site of AChBP [17,18]. This suggests that AChBP and nAChRs share similar functional and structural properties [13,19], and that AChBP may serve as useful structural templates for comparative modeling of the ECDs of nAChRs.

Conotoxins, derived from marine cone snail, are peptides rich in disulfide bonds connecting conserved cysteine residues. The synthesis and manipulation of these neuroactive peptides as potential pharmacophores and molecular probes have attracted attention because of their relatively short length, well-defined backbone structure, and specificity to a wide range of ion channels and nAChRs with high potency [1,20–22]. Furthermore, with many possible variations of amino acid residues apart from conserved cysteines, conotoxins vary greatly in their ability to target different neuronal/muscular acetylcholine receptors [23]. The most studied conotoxin subfamily is α -conotoxins, that are known to naturally and selectively bind at nAChR subtypes that modulate the cholinergic pathway [24], as mentioned previously. α -Conotoxins commonly contain fewer than 20 amino acid residues with a compact structure including 2 disulfide bridges [25]. These peptides are widely utilized to probe the structure-function relationships of nAChR binding sites [26], for differentiating variable nAChR subtypes [5], and in the development of potential pharmacological tools [27].

α -conotoxin LsIA (17 amino acids in length), is a neuropeptide discovered from *Conus limpusi*, which shows distinct high binding affinity ($IC_{50} = 10.1$ nM) for targeting human (h) $\alpha 7$ nAChR subtype relative to $\alpha 3\beta 4$ [28], $\alpha 3\beta 2$ and $\alpha 3\alpha 5\beta 2$ nAChR subtypes, as determined in previous experiments [29]. Similar to other α -conotoxins, LsIA possesses 2 disulfide bonds connecting 4 conserved cysteine residues [30], and the disulfide bridges produce a unique 2-loop structure (4/7) [23] with a naturally amidated C-terminal (shown in Figure 1A). The unique motif in loop 1 of certain α -conotoxins was implicated in subtype-selective binding to nAChRs via the highly conserved proline [31], such as Lo1a, GID and LsIA (in position 7 in LsIA) [1,29,32]. Other studies also pinpointed the importance of residues in the loop 2 on the specificity of α -conotoxins binding at nAChRs [33]. Moreover, it has been demonstrated that the C-terminus, ARG10 and connective ASNs (in position 12 and 13) of LsIA are involved in distinguishing between neuronal subtypes, namely, $\alpha 3\beta 4$ [28], $\alpha 3\beta 2$ and $\alpha 7$ nAChR [29], with mutations based on these residues showing distinct efficacies. It has also been shown that carboxylation of the C-terminus of α -conotoxin LsIA reduces potency to human $\alpha 7$ nAChR relative to naturally amidated LsIA, but enhances potency at $\alpha 3\beta 2$ [29], highlighting the potential efficacy of C-terminus modification to alter nAChR subtype selectivity. Additionally, apart from most α -conotoxins, some peptides from other conotoxin subfamilies also retain a naturally amidated C-terminal, such as μ -conotoxin GIIIA [34] and KIIIA [35], ω -conotoxin, CVID [36] and MVIIA [37] that target ion channels and other proteins. Among them, MVIIA (ziconotide), is a strong analgesic for treating severe chronic pains, which has been approved by the US Food and Drug Administration (FDA) [38], meanwhile other conotoxins, such as ω -CVID [36] and α -Vc1.1 [39] for treatment of neuronal and cancer-related pains [40] are under clinical trials [41,42]. The possibility of altering the selectivity or potency via C-terminal carboxylation of these conotoxins, of known therapeutic importance, provides an additional exciting avenue for the development of novel conotoxin derivatives which may serve as molecular probes or new treatments.

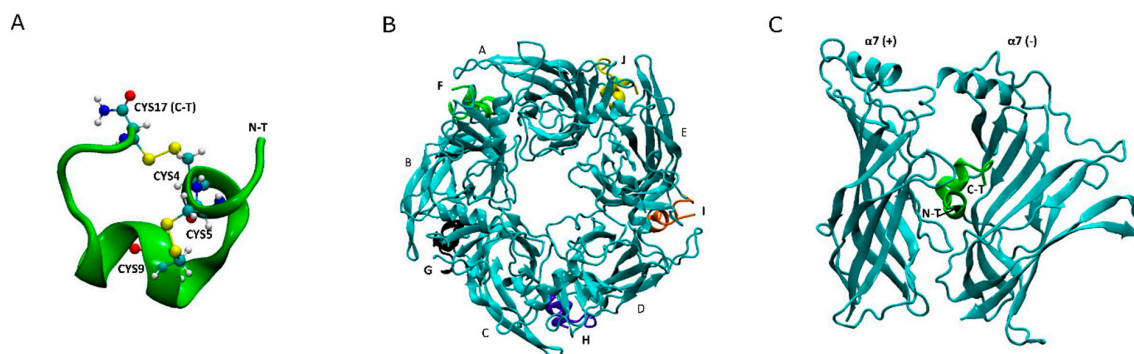


Figure 1. Ribbon conformation of amidated LsIA binding to human $\alpha 7$ nAChR. **(A)** The conformation of LsIA with four conserved cysteines. **(B)** Top view of LsIA binding at five interfaces between adjacent $\alpha 7$ subunits, where the subunits are shown in *cyan* color. **(C)** Side view of LsIA anchored to one interface of two adjacent $\alpha 7$ subunits.

Previous studies have mainly provided insights into determinants that affect the binding of some α -conotoxins to human $\alpha 7$ nAChR, in order to better understand the binding mechanisms of ligands [23,43], and structure-function relationships of $\alpha 7$ nAChR and α -conotoxins [1,44]. Additionally, much work has focused on mutating and synthesizing novel neuropeptides binding at the receptors with improved efficacy and specificity, experimentally or proposed via computational predictions [21,26,29,45].

It is widely accepted that α -conotoxins bind at the interface between two adjacent $\alpha 7$ subunits [18,46–48], where aromatic pockets are present for ACh targeting [49]. One example of binding conformation of α -conotoxin LsIA to human $\alpha 7$ nAChR is shown in Figure 1B,C. Compared with AChBP, highly conserved amino acids of $\alpha 7$ nAChR are contained within 7 loops, for which 3 loops (A–C) are located on the principal face, also termed the (+) face, and 4 loops (I–IV) on the complementary face, denoted as the (–) face [43], constituting the binding site of the ECD of $\alpha 7$ nAChR [50]. The key residues of these loops, therefore, play significant roles in interactions with key residues of α -conotoxins. The most important residue pairs that affect the stabilization of human $\alpha 7$ and α -ImI complex and human $\alpha 7$ and α -PnIB conformation are ImI-ARG7 and $\alpha 7$ -TYR217(+), and PnIB-LEU10 and $\alpha 7$ -TRP171(+) [23,43], via cation- π and hydrophobic interactions respectively. In contrast, residues on the complementary interface of rat $\alpha 7$ subunit exert a pivotal impact on the binding affinity of α -conotoxin TxIA (A10L) [51], and residues at the (–) face of human $\alpha 7$ nAChR are also implicated in the determination of selectivity of α -conotoxins to the receptors [23]. Furthermore, in recent studies, Abraham and et al. determined the co-crystal structure of *Lymnaea stagnalis* (Ls) AChBP and LsIA complex [28]; and which was used as the template for building comparative models of LsIA bound to human $\alpha 7$, $\alpha 3\beta 2$ and $\alpha 3\beta 4$ complexes. However, a gap in the knowledge exists regarding the important role of the C-terminal of α -conotoxins in their selectivity and stabilization to nAChRs at the atomic level, and needs further investigation in order to understand and fully exploit the potential of C-terminal modification in designing novel conopeptides for nAChR selective probes and potential drug leads.

In the present study, we elucidate the interaction mechanism of both amidated LsIA and carboxylated C-terminal of LsIA with human $\alpha 7$ using molecular dynamics (MD) simulations together with a number of computational analysis methods. We identified unique intramolecular interactions within LsIA which favored particular conformational motifs for amidated type LsIA, thereby facilitating unique interactions with respective residues of the LBD of $\alpha 7$ nAChR which are absent in carboxylated LsIA. Key pairs of residues have been investigated which are known to be highly implicated in the enhancement of binding potency of amidated LsIA targeting $\alpha 7$ nAChR, compared with its LsIA analogue bound form. We also employed an inter-residue contact network analysis approach for determination of possible disruptions or changes to inter-subunit interactions due to binding of

amidated and carboxylated LsIAs, and proposed additional possible structural characteristics which may be related to the higher potency of amidated LsIA relative to carboxylated LsIA.

2. Results and Discussion

2.1. Homology Modeling of Amidated and Carboxylated LsIAs Anchoring to Human $\alpha 7$ nAChR

The starting homology models of $\alpha 7$ /LsIA were constructed using 2BR8 as a template, and subsequently simulated. We note that a recent co-crystal structure is available of *Lymnaea stagnalis* AChBP (*Ls*-AChBP) bound to amidated α -conotoxin LsIA (PDB code: 5T90 [29]), which showed minor structural differences in AChBP compared to all other conotoxin-*Ac*-AChBP crystal structures to date, possibly due to species differences between *Ls*- and *Ac*-AChBP. The authors constructed homology models of amidated LsIA bound to $\alpha 7$ nAChR based on *Ls*-AChBP, and comprehensively elaborated and tested key interactions identified in the model in a number of elegant experiments. Nonetheless, the minor structural differences between *Ls*- and *Ac*-AChBP, and the availability of co-crystal structures of 4/7-conotoxins bound to both species isoforms, afford an opportunity to explore an alternative, possible conformation of LsIA- $\alpha 7$ complex based on *Ac*-AChBP, which shares a comparable (though somewhat lower) sequence similarity to human $\alpha 7$. In this work, we compare and contrast the present LsIA- $\alpha 7$ model based on *Ac*- to that based on *Ls*-AChBP where relevant.

2.2. Amidated LsIA Binding Causes Higher Fluctuations in Loop C and the Juxtamembrane Cys-Loop Regions

Time series plots of RMSD, calculated for the backbone atoms and averaged over 12 simulations, for amidated and carboxylated LsIA- $\alpha 7$ nAChR complexes, are shown for the $\alpha 7$ subunits in Figure 2A,B, and for the LsIA toxins in Figure 2C,D. These RMSD plots are qualitatively similar to those of previous simulations of nAChRs-toxins complexes [14,18,52]. The structure of amidated LsIA (Figure 2C) and human $\alpha 7$ nAChR (Figure 2A) complex becomes stabilized, on average, after 20 ns, while the carboxylated LsIA binding at the extracellular domain (ECD) does not achieve its stabilization until 27 ns (Figure 2B,D), and appears to continue to exhibit structural drift towards the end of the simulation period. Thus, there is greater variation in the RMSD plots for the carboxylated LsIA- $\alpha 7$ system compared to amidated LsIA, suggesting that the carboxylated LsIA- $\alpha 7$ complex might be somewhat less stable. This demonstrates a potentially more stable structure of amidated LsIA binding to $\alpha 7$ nAChR complex. This is discussed further in the sections below.

However, the RMSD results show an asymmetric pattern in chain H in amidated LsIA (Figure 2C), which demonstrates a divergent pattern with higher RMSD values (around 0.425 nm) versus the other 4 chains of LsIA, whereas there is no such pattern present in the carboxylated counterpart (Figure 2D). Thus, the amidated LsIA-bound form provides a more steady structure over its analogue binding complex, while the rigidity of protein structure varies in distinct portions of the protein complex (Figure 2C,D). The RMSD plot of chain H (ligand) in amidated LsIA is different from the other chains of the amidated LsIA (Figure 2C). This may suggest a potentially distinct interaction between chain H and corresponding ligand binding domain (LBD) compared with the others. By contrast, we did not observe substantial differences between the five carboxylated LsIA toxins (Figure 2D), nor is there any substantial difference among the chains of $\alpha 7$ nAChR bound by amidated and carboxylated LsIAs (Figure 2A,B). Overall, the RMSD results indicate that amidated LsIA- $\alpha 7$ reach stability earlier, with less fluctuation in RMSD per chain compared to carboxylated LsIA- $\alpha 7$. However, for the amidated complex, there is some asymmetry in the RMSD, with one of the LsIA monomers in the amidated complex undergoing substantially higher structural deviation compared to the others, likely due to LsIA N-terminal (N-T) fluctuations (see below). A similar asymmetric pattern also occurred in the RMSD plot of apo chicken $\alpha 7$ nAChR, determined by Yi and colleagues [15]. RMS fluctuation (RMSF) plots are shown for the amidated and carboxylated LsIA-bound $\alpha 7$ receptor residues in Figure 2E,F, and for the toxin residues in Figure 2G,H, respectively. The absolute RMSF values for the $\alpha 7$ receptors (Figure 2E,F) for both amidated and carboxylated bound forms are consistent with previous studies on

human $\alpha 7$. These plots demonstrate the greatest flexibility in the Cys-loop, and are similar to the RMSF results of several previous studies, such as that of α -ImI bound form, by Yu et al. via computational simulations [18], who found that the Cys-loop RMSF increased compared with apo human $\alpha 7$ nAChR. There is also relatively high flexibility of $\beta 1/\beta 2$ loop and $\beta 10$ strand, similar to previous studies [53].

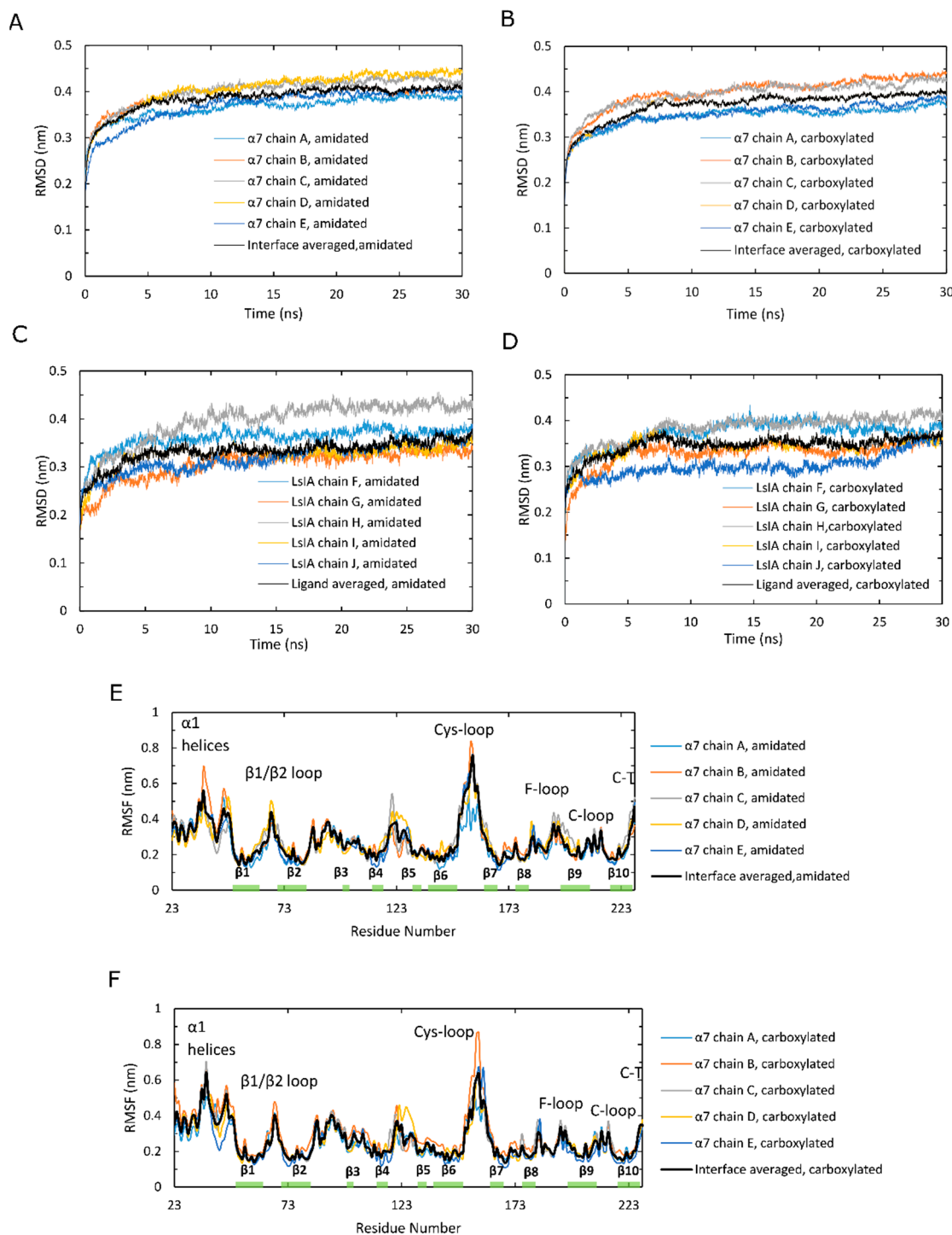


Figure 2. Cont.

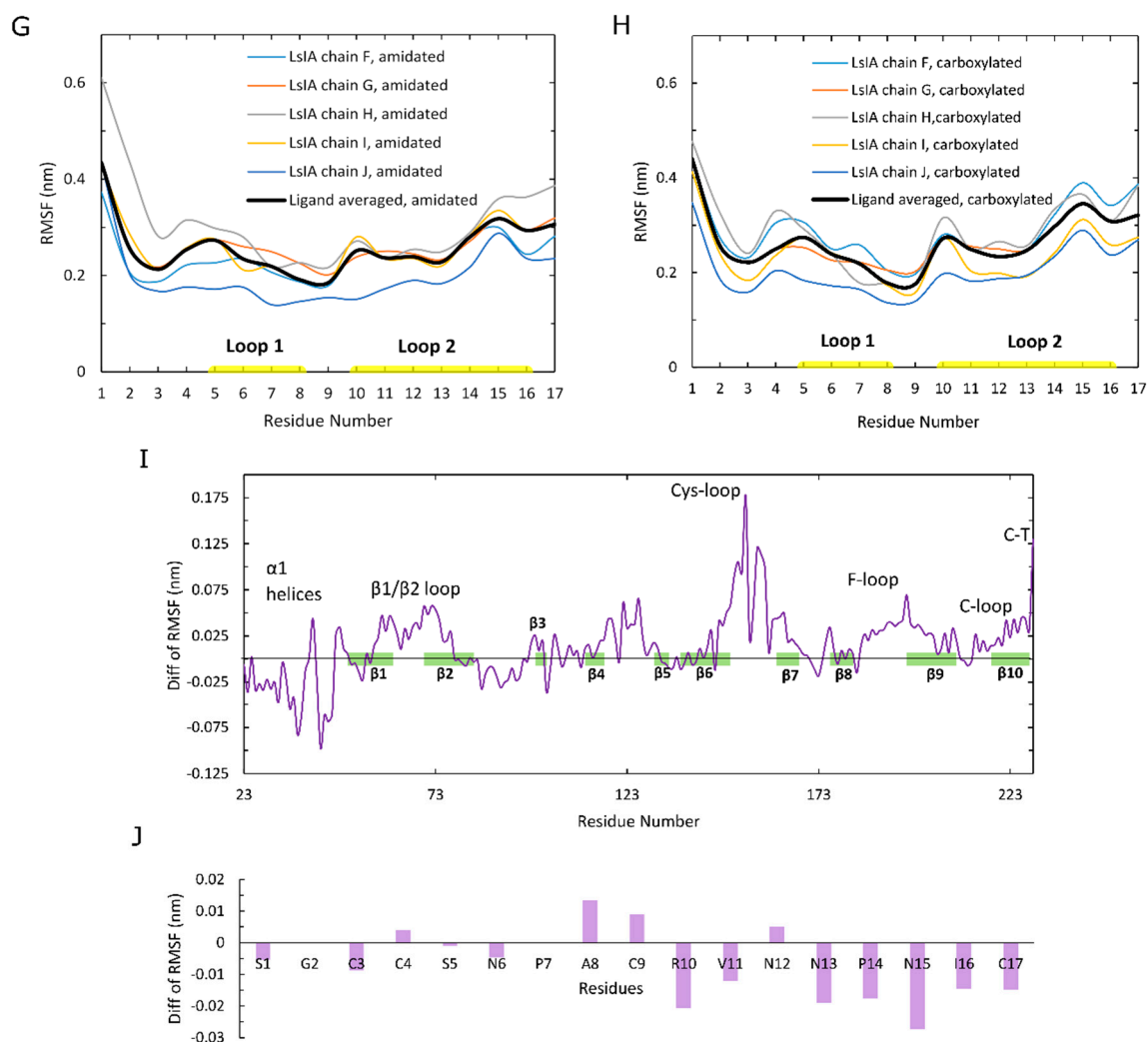


Figure 2. Analysis of stability of human $\alpha 7$ nAChR over molecular dynamics (MD) simulations in the amidated (wt) LsIA and C-terminal carboxylated (mut) LsIA bound types. (A,B) C α atoms in β strand RMSD of five $\alpha 7$ subunits in the wt-LsIA and mut-LsIA bound forms, respectively. (C,D) C α atoms in β strand RMSD of five ligands (LsIA) binding in the ligand binding domain (LBD) in the wt-LsIA and mut-LsIA, respectively. (E,F) C α RMSF of five $\alpha 7$ subunits in the wt-LsIA and mut-LsIA bound forms, respectively. (G,H) C α RMSF of five ligands (LsIA) binding in LBD in the wt-LsIA and mut-LsIA, respectively. The black curves demonstrate the mean values of RMSD/RMSF of the five interfaces/ligands in the LsIA binding complexes. (I) Differences of C α RMSF between wt-LsIA and mut-LsIA bound $\alpha 7$ subunits. (J) Differences of C α RMSF between wt-LsIA and mut-LsIA (amidated mean subtracts carboxylated mean).

In order to clearly show the differences in $\alpha 7$ receptor residue RMSF when bound to amidated compared to carboxylated LsIA, Figure 2I shows “Diff in RMSF”, taken by subtracting the receptor RMSF values of the carboxylated complex from those of the amidated complex. Thus, for example, residues with positive “Diff in RMSF” values indicate higher flexibility for amidated relative to carboxylated LsIA- $\alpha 7$ complex. The main difference is that there is substantially higher flexibility in the Cys-loop region for amidated compared to carboxylated LsIA. This region forms the main contact between the ECD and transmembrane domain (TMD; though absent in the present simulation) in the full $\alpha 7$ nAChR. Enhanced flexibility in the Cys-loop regions could be related to changes in $\alpha 7$ channel activity, and could provide an indirect measure of the potential inhibitory effects of conotoxins bound to nAChR ECDs. Further work involving the whole $\alpha 7$ receptor bound to conotoxins will likely be required to examine the direct impact of toxin binding on the pore region. Another region that exhibits

marginally higher RMSF for amidated LsIA-bound $\alpha 7$ is the loop C region, which forms part of the canonical agonist binding site and, in the α -subunits of nAChRs, is composed of a β hairpin with a twin Cys motif at the edge of the loop. This enhanced fluctuation is in accordance with previous studies on nAChRs, including those for apo $\alpha 7$ and $\alpha 7$ -antagonist-bound complexes [53]. Nonetheless, the higher RMSF of both loop C and the juxtamembrane Cys-loop region, for amidated LsIA, is consistent with the present notion that movements in these two areas are strongly coupled, and is required for transmission of structural effects due to agonist (or antagonist) binding from the ECD to the transmembrane pore. The higher RMSF for both these regions for amidated LsIA suggests that this natural form of the conotoxin may have a greater impact on the ligand binding and subsequent TMD coupling mechanism of $\alpha 7$ compared to the less potent, carboxylated form.

There are also slightly higher RMSF values in regions of the $\beta 1/\beta 2$ loop and C-terminus of $\beta 10$ strand that are related to pore gating in the TMD. Both regions are related to the contacts between ECD and TMD for mediating the open and closed states of the pore in TMD, but via distinct pathways. The increased flexibility of the former regions that interact with M2–M3 linker may cause a conformational change of M2 α -helices in the TMD [54–56], which is a known role of the Cys-loop in pore gating of Cys-loop receptors [57,58]. The latter region is associated with the N-terminus of M1 in the TMD via covalent interactions [59].

Additionally, there is reduced flexibility in the N-terminal $\alpha 1$ helices of nicotinic $\alpha 7$ nAChR bound by amidated LsIA relative to carboxylated LsIA. This region has been demonstrated to form a key Fab35 antibody binding region for muscle-type nAChR subtype [60], but its role in neuronal nAChRs is presently less clear. The impact of conotoxin binding on nAChR-antibody linkage is an intriguing future avenue of research. The absolute RMSF plots for the toxin residues of amidated and carboxylated LsIAs are shown in Figure 2G,H respectively. Both exhibit similar patterns of RMSF, with especially high fluctuation at N- and C-terminal residues. As with the RMSD behavior described above, for amidated LsIA, there is some asymmetry in RMSF, with one monomer (labeled chain H in Figure 2G) exhibiting substantially higher fluctuation in the N-terminus compared to all four of the other monomers. Thus, the source of asymmetry appears to be localized mainly to the disordered and highly flexible loop 1 residues, SER1 and GLY2.

To directly compare the effects of carboxylation, the “Diff in RMSF” plot for the LsIA residues is shown in Figure 2J. It can be seen that residues ALA8 and CYS9 are more flexible for the amidated LsIA, with positive “Diff in RMSF” values. However, the main impact is that amidated LsIA has a more rigid structure in residues of loop 2 (except for ASN12) and in the N-terminus of LsIA (Figure 2G,H,J). The rigidity in loop 2 is due to differences in both toxin-receptor complexes, as well as intramolecular LsIA contacts, as detailed below.

2.3. Carboxylation at LsIA C-Terminus Causes Indirect Loss of Contacts between Key Residue ARG10 and the $\alpha 7$ Complementary Face

To explain differences in RMSD and RMSF, we examined how amidation and carboxylation change the extent of residue pairwise contacts between LsIA and $\alpha 7$. Figure 3A shows the absolute total number of contacts between each residue of amidated (green) and carboxylated (pink) with $\alpha 7$, as well as differences (amidated minus carboxylated, Figure 3B). The most significant interactions formed by amidated and carboxylated LsIAs with $\alpha 7$ subunit, which predominantly occurred in ARG10 and VAL11 in loop 2 and LsIA-PRO7 in loop 1, which is also known to exert a great impact on selective targeting by the ligand (Figure 3A) [28,61]. Other minor interactions are established by LsIA-CYS17 and the residues on the receptor, significantly contributing to the contacts of LsIA (Figure 3A,B). In contrast, although LsIA-ALA8 makes substantial contacts with the receptor, its impact on selectively binding to the target is much lower when compared with other residues of LsIA, as explained below.

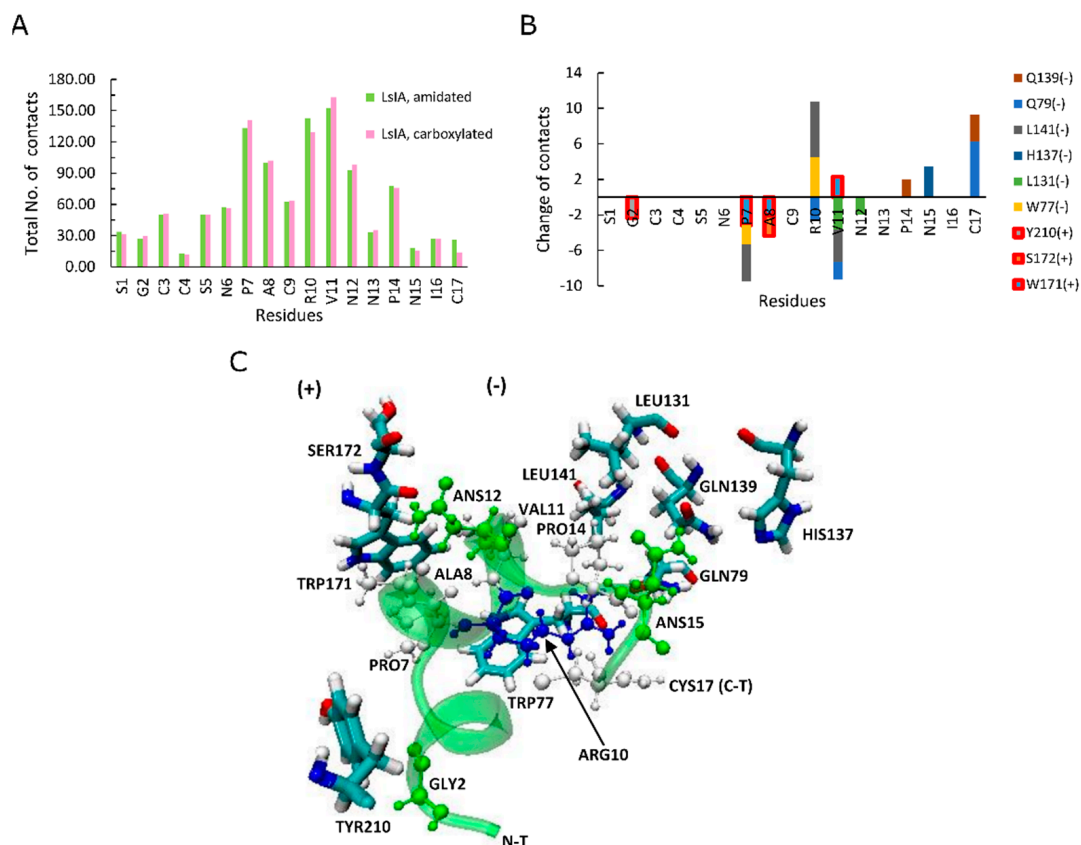


Figure 3. A total number of contacts and the variations between amidated (wt) LsIA and C-terminal carboxylated (mut) LsIA bound types. (A) The total number of contacts for amidated (green) and carboxylated (pink) LsIA with human $\alpha 7$ nAChR. (B) The significant changes (Amid minus Carb) in the number of contacts between wt-LsIA and mut-LsIA bound types. (C) The interactive residues of the wt-LsIA and the $\alpha 7$ nicotinic receptor complex.

Figure 3B shows differences in the number of contacts for the LsIA residues. The effects of gaining contacts for amidated, relative to carboxylated LsIA, outweighed those of losing contacts on the LBD of human $\alpha 7$ nAChR subtype in total, as also suggested by Inserra et al. in their experimental results [29]. However, there were no significant changes appearing in loop 1 of LsIA, while most of the variations of contacts took place in loop 2 and C-terminus of LsIA (Figure 3B). Since loop 2 makes contacts mostly with $\alpha 7(-)$ (Figure 3B,C), this pattern indicates that the CT amidation/carboxylation state mainly affects interactions with the $\alpha 7(-)$ face. Enhancement in toxin-receptor contacts for the amidated form is qualitatively consistent with this toxin's higher potency compared to the carboxylated form. Two residues in loop 2 show substantially higher contacts for the amidated form; ARG10 and CYS17 (Figure 3B). This is consistent with the predicted importance of ARG10 in forming close hydrogen bonds with the hydrophilic pocket of $\alpha 7$ in previous recent studies [28]. Compared with the carboxylated LsIA bound form, although wt-LsIA-ARG10 shows a higher absolute number of contacts with $\alpha 7$ nAChR, in relative (percentage) terms, wt-LsIA-CYS17 has the greatest enhancement, with an increase of 45% higher contact number compared with the other residues of amidated LsIA (not shown). On the contrary, the most significantly impaired interaction was attributed to GLY2 with around 20% decrease (not shown). Additionally, PRO7, VAL11 and ASN12 show minor reductions for amidated LsIA and $\alpha 7$ nAChR complex, but the contacts of ASN in position 15 and PRO14 with the receptor are slightly enhanced in the amidated ligand-bound form. Overall, then, for the amidated LsIA, an increase in the number of contacts at ARG10 and the C-terminus with $\alpha 7$ (Figure 3B) is likely responsible for its higher rigidity in loop 2 (Figure 2J, RMSF plots) compared to the carboxylated form. Since ARG10 is known to be a key residue responsible for LsIA inhibition of nAChRs [28], our present simulation

results indicate that introducing a negative charge via carboxylation at the C-terminus not only causes reduction in contacts directly with CYS17, but also an indirect loss of contact at ARG10, and this latter disruption may play the key role in lower potency of the carboxylated LsIA at $\alpha 7$.

2.4. Amidated LsIA Favors Hydrogen Bonding and π - π Interactions between ARG10 and the $\alpha 7(-)$ Subunit

We examined specific toxin-receptor pairwise contacts, which may play an important role in improving the selectivity of amidated LsIA binding to human $\alpha 7$ nAChR, namely LsIA-CYS17 with $\alpha 7$ -GLN79(-) and GLN139(-), and LsIA-ARG10 with $\alpha 7$ -LEU141(-) and TRP-77(-) (Figure 3C). In contrast, PRO7 and VAL11 of carboxylated LsIA possess preferential contacts with residues on the principal (+) face of $\alpha 7$. We first discuss interactions which favor the amidated LsIA, followed by those that favor carboxylated LsIA.

For amidated LsIA, a significant interaction is established between LsIA-ARG10 and $\alpha 7$ -TRP77(-) and LEU141(-) via hydrogen bonds and cation- π interaction, respectively, via a sandwich-like arrangement (Figure 4A), which was observed in the amidated but not carboxylated (Figure 4A,B), LsIA. Compared with the carboxylated analogue and $\alpha 7$ nAChR complex, a unique sandwich-like conformation [62], composed by wt-LsIA-ARG10 and $\alpha 7$ -TRP77(-) (3.9 Å) and $\alpha 7$ -LEU 141(-) (1.7 Å/2.9 Å) (Figure 4A), was determined, and this group of interactions might serve to stabilize interaction of ARG10 with residues at $\alpha 7(-)$, leading to a deeper burial of amidated LsIA into the binding pocket. A similar 'sandwich' motif has also been determined by Grishin and colleagues through computational methods [63], demonstrating a particular arrangement for AulB-F9 and aromatic residues, LYS61 and TRP59, in the $\beta 4$ subunit of $\alpha 3\beta 4$ nAChR. However, the interactions involved in the present study also include hydrogen bond formation.

We also observed a perpendicular (T-shaped) position of the LsIA-ARG10 sidechain with respect to $\alpha 7$ -TRP77(-) in both LsIA bound conformations (Figure 4C,D), wherein both cation- π interactions are likely to be relatively weak in this arrangement (4.0 Å in amidated LsIA; 5.0 Å in carboxylated LsIA). The intramolecular interactions between CYS4 and ARG10 may account for this situation, as this T-shaped motif often occurred when LsIA-CYS4 lost its persistent contacts with the guanidinium moiety of ARG10. Nevertheless, this perpendicular conformation is relatively rare in the wt-LsIA bound form, due to the tight intramolecular interactions.

Furthermore, the cation- π interaction has also been demonstrated between ARG7 of α -ImI and aromatic residues, such as TYR217(+), TRP171(+) and TYR115(+), on the binding pocket of human $\alpha 7$ nAChR through computational docking results [64]. In addition, as TRP77(-) significantly affected the specific binding of α -ImI to human $\alpha 7$ nAChR and was shown to be crucial for modulating the response of rat $\alpha 7$ nAChR to the existence of agonist [43,65], further investigation on binding of LsIA at human $\alpha 7$ nAChR may help to explicate the important role of TRP77(-) in LsIA binding. The preferential interactions involving hydrogen bonding between ARG10 and the hydrophilic environment of the $\alpha 7(-)$ subunit is in qualitative agreement with the model proposed by Abraham et al. [28].

Other, more minor interactions identified in the present simulations include those between the amidated-LsIA-CYS17 with GLN139(-) and GLN79(-) (Figure 5A,B) as well as HIS137(-) (not shown), of $\alpha 7$ subunit, via hydrogen bond interactions. Notably, interactions between CYS17 and the respective GLN residues of the receptor, are amongst the most significantly enhanced contacts, compared with its carboxylated counterpart bound complex (Figure 3B). However, it should be noted that although the distance between amidated LsIA-CYS17 and GLN139(-) is decreased, the interaction between them is likely to be relatively weak, as a hydrogen bond interaction is not possible due to a long distance (8.6 Å) between LsIA-CYS17 and GLN139(-). The proximate packing of wt-LsIA (Figure 5C) allowed a minor persistent hydrogen bond interaction between contacts of PRO14 and GLN139(-) (1.8 Å/3.3 Å) (Figure 5B,D), whereas a relatively weak van der Waals interaction is established with corresponding residues in the carboxylated LsIA binding form (Figure 5A).

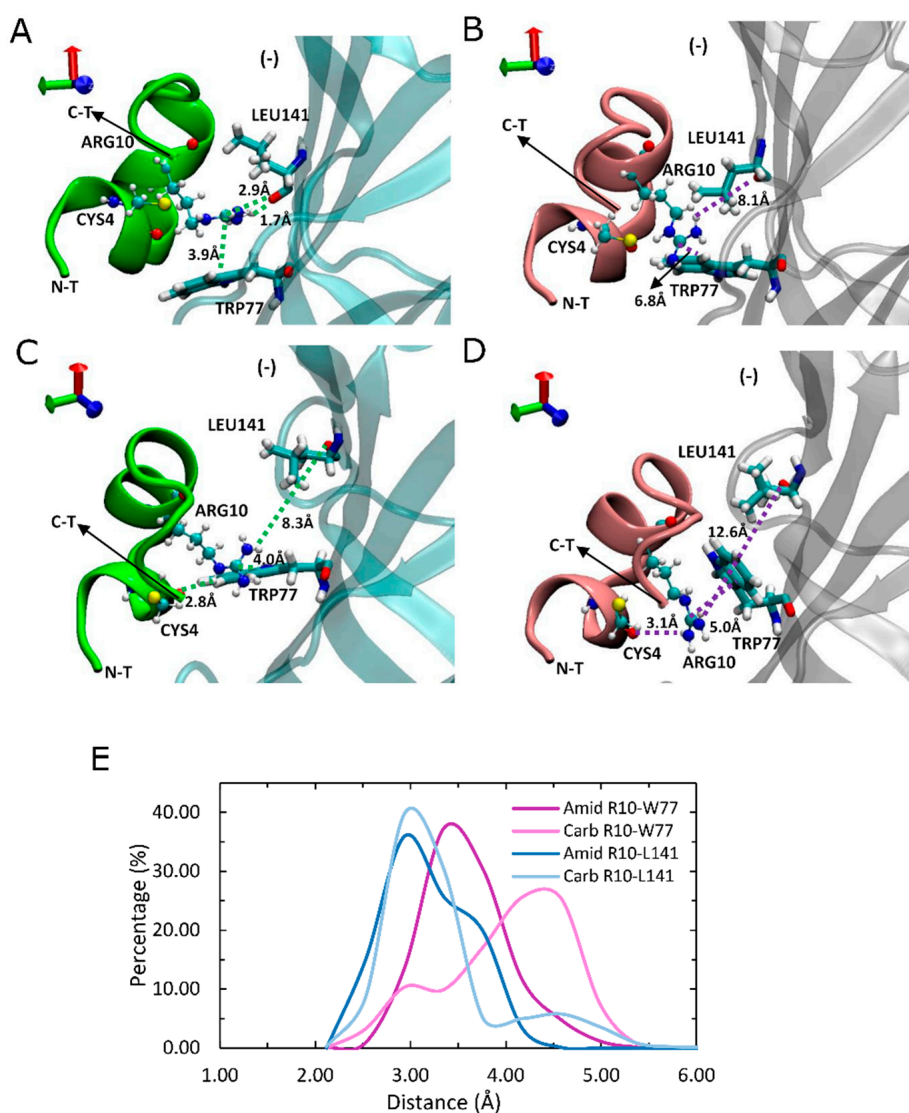


Figure 4. Side view of binding conformation of LsIA-ARG10 to the ligand binding domain (LDB) of human $\alpha 7$ nAChR. (A) The sandwich-like motif of amidated (wt) LsIA-ARG10 with $\alpha 7$ -LEU141(-) and TRP77(-) and (B) binding conformation of carboxylated (mut) LsIA with corresponding residues. (C,D) Perpendicular-like binding conformation of LsIA-ARG10 with $\alpha 7$ LEU141 and TRP77 in amidated (C) and carboxylated (D) LsIA bound form, respectively. The purple and green dash lines indicate the residues of LsIA with impaired and improved interaction with respective residues of the receptor, respectively, whereas the receptor subunits bound by wt-LsIA (green) and mut-LsIA (pink) are shown in transparent cyan and silver colors, respectively. (E) Distances (Å) of the corresponding interactions between residues of LsIA and receptors in ligand-bound forms via gmx_mindist.

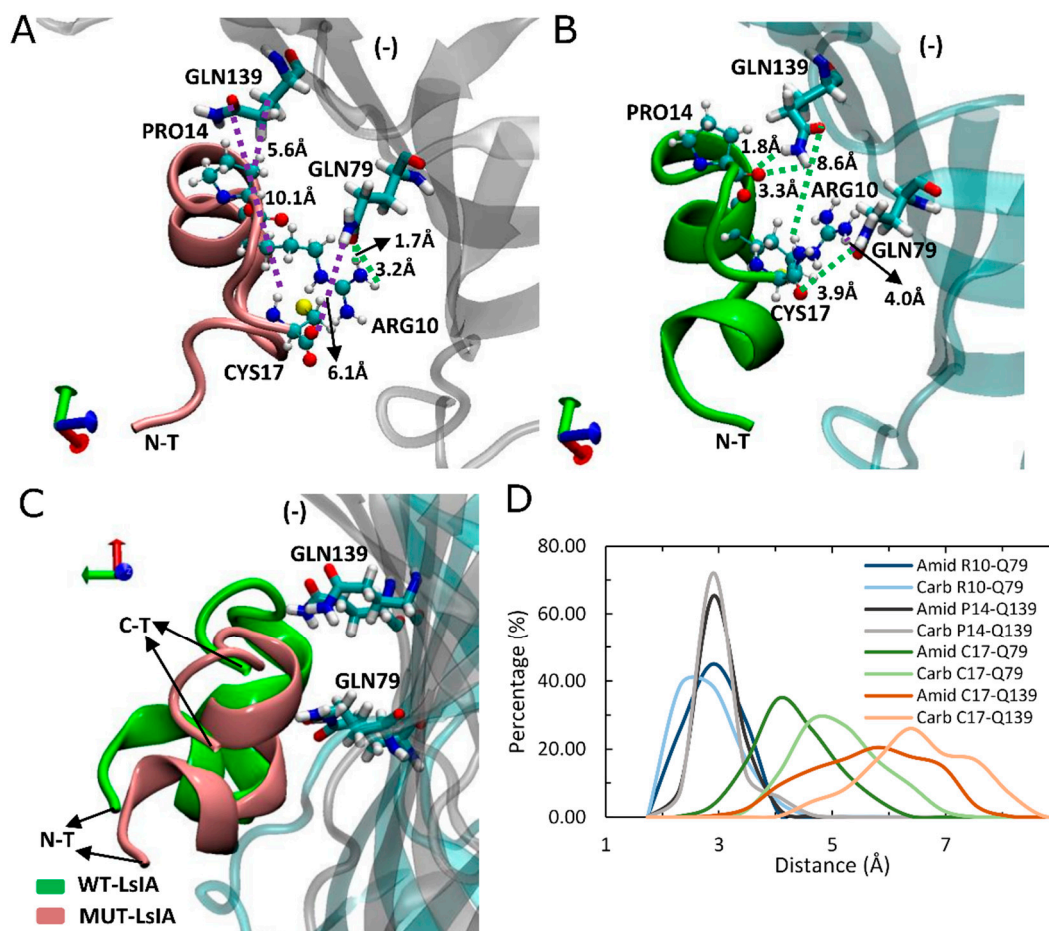


Figure 5. Binding model of LsIA-PRO14, ARG10 and CYS17 of amidated (wt) LsIA and C-terminal carboxylation (mut) LsIA into the binding pocket on the complementary (–) face of human $\alpha 7$ nAChR. (A,B) Interactions established by ARG10, PRO14 and CYS17 with corresponding residues in amidated (green) and carboxylated (pink) LsIA binding forms. (C) Side view of the binding conformation of the wt-LsIA and mut-LsIA to $\alpha 7$ nAChR subunit. (D) Distances (Å) of the corresponding interactions between residues of LsIA and receptor in ligand-bound forms.

2.5. Carboxylated LsIA Favors Hydrophobic Interactions with $\alpha 7$ Subunit Residues via PRO7 and VAL11

The description in the above section noted the loss of amidated LsIA contacts between PRO7 and ALA8 with $\alpha 7$ -TRP171(+), and VAL11 with $\alpha 7$ -LEU131/141(–) (Figure 3B) which are, conversely, favored by the carboxylated LsIA. This may be related to the shifting of the balance in LsIA interactions with the principal (+) and complementary (–) subunits mentioned above.

In addition to $\alpha 7$ -TRP171(+) having higher contacts with carboxylated LsIA-PRO7 and LsIA-ALA8 (Figure 6), we noted that the interaction between TRP171(+) and LsIA-PRO7 also shows the highest absolute number of contacts in both amidated and carboxylated LsIA bound receptors (not shown). Proline in position 7 of LsIA, which is amongst the conserved amino acids of LsIA, played a critical role in the formation of the α -helix structure of α -conotoxins, by strongly contributing to binding of α -conotoxins at nAChR receptor through making various contacts with residues on both sides of the binding site [1,43,64]. From the inter-residue contact results, the highest number of contacts are formed between $\alpha 7$ -TRP171(+) and carboxylated LsIA-PRO7 due to hydrophobic interaction between TRP171(+) and the imino ring of carboxylated LsIA-PRO7, the interaction of which has also been identified between $\alpha 7$ -TRP171(+) and PnIB-PRO6 and PRO7 in previous experimental studies of other conotoxins [4,23]. Furthermore, VAL11 forms hydrophobic contacts with the residues LEU131/141(–), further contributing to enhanced hydrophobic interactions relative to amidated LsIA.

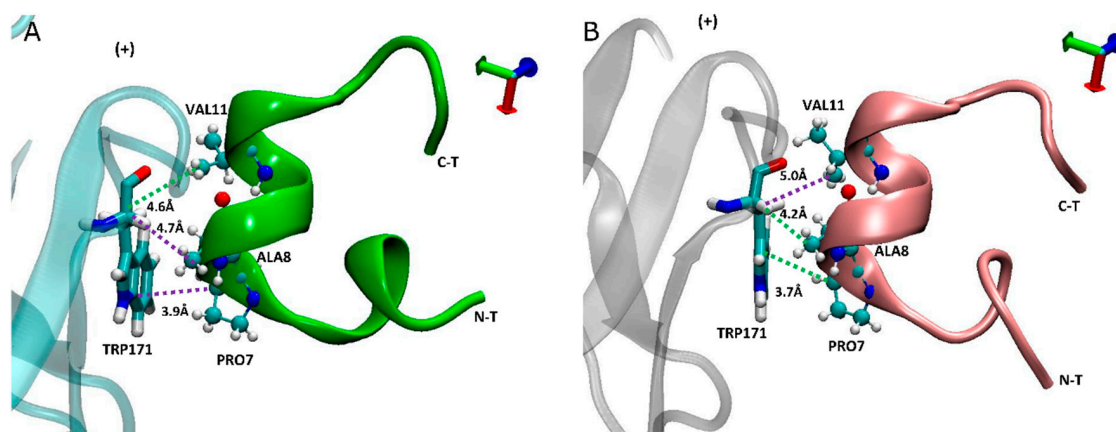


Figure 6. Side view of binding conformation of LsIA into the binding pocket with the interaction between human $\alpha 7$ -TRP171(+) and LsIA-PRO7, ALA8 and VAL11, respectively. **(A)** The conformation of amidated LsIA anchored to the principal (+) face of $\alpha 7$ subunit. **(B)** The conformation of carboxylated LsIA anchored to the (+) face of $\alpha 7$ subunit.

2.6. $\alpha 7$ -TYR217 Forms Close Contacts with Both Amidated and Carboxylated LsIAs

As the principal determinant for binding of ImI is the interaction between aromatic ring of $\alpha 7$ -TYR217(+) of receptor and ARG6 [43], we also investigated the interaction between $\alpha 7$ -TYR217(+) and respective residues of LsIA. However, there is no potential interaction between LsIA-ARG10 of amidated or carboxylated LsIA and the corresponding residue; nor are apparent variations of interactions between these two residues detected, due to the position of LsIA-ARG10 being relatively far away from $\alpha 7$ -TYR217(+) (Figure 7A,B). Nonetheless, several contacts were identified in the present simulations, between $\alpha 7$ -TYR217(+) and LsIA-ALA8, LsIA-CYS9 and the two ASN residues in loop 2 of the toxin, which were observed in both amidated and carboxylated LsIAs. Among them, the most notable interaction is established by LsIA-CYS9 with $\alpha 7$ -TYR217(+). CYS9 is in close proximity with TYR217(+), which allows van der Waals interaction that could be an important determinant for binding LsIA at $\alpha 7$ nAChR (Figure 7A,B). Additionally, hydrophobic interaction formed by $\alpha 7$ -TYR217(+) and LsIA-ALA8 also may be related to the anchoring of LsIA and its variant to human $\alpha 7$. However, there are no obvious changes in contacts between TYR217(+) and CYS9 regarding carboxylating the C-terminal of LsIA, whereas the degree of hydrophobic interaction between LsIA-ALA8 and TYR217(+) (3.9 Å) is slightly higher in amidated LsIA receptor complex compared with the carboxylated LsIA (6.2 Å) (Figure 7). In contrast, the van der Waals interaction established between LsIA-GLY2 and $\alpha 7$ -TYR210(+) is reduced, possibly owing to the amidated LsIA being more deeply inserted into ligand binding pocket, together with a more flexible backbone of the N-terminal of amidated LsIA, relative to its carboxylated analogue bound form.

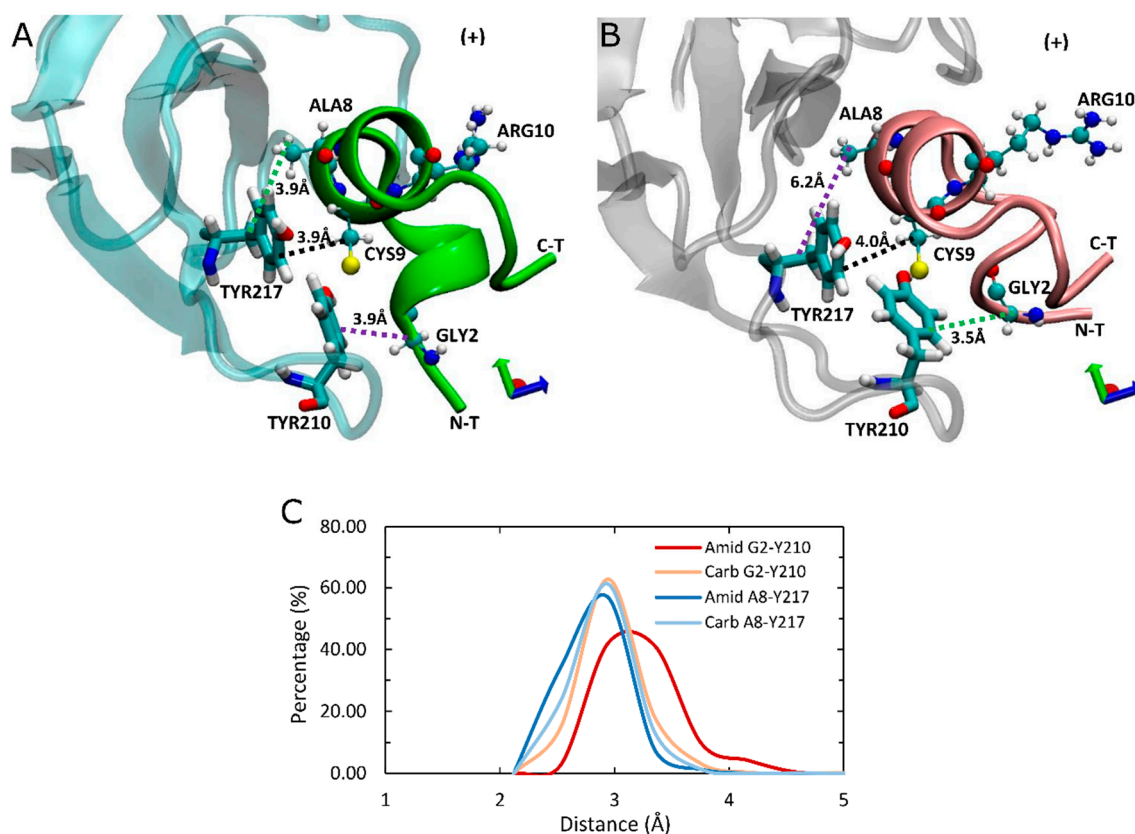


Figure 7. Top view of binding conformation of amidated (wt) and carboxylated (mut) LsIA at the principal (+) face of human $\alpha 7$ nAChR. **(A)** The conformation of wt-LsIA anchored to the (+) face of $\alpha 7$ subunit. **(B)** The conformation of mut-LsIA anchored to the (+) face of $\alpha 7$ subunit. The black dash lines demonstrate the interaction occurred in both LsIA bound forms. **(C)** Distances (Å) of the interactive residues in LsIA and the LBD of $\alpha 7$ nAChR complexes.

2.7. An Intramolecular Salt-Bridge in Carboxylated LsIA Is Retained Upon Binding to $\alpha 7$, and Plays a Role in the Loss of Key Toxin-Receptor Contacts

While C-terminal amidation is known to be important for the folding of α -conotoxin ImI through its effects on disulfide pairing [66], it may also directly or indirectly affect the binding stability of LsIA to human $\alpha 7$ nAChR via intramolecular interactions. The present simulations indicate that the carboxylated LsIA-CYS17 forms a stable salt bridge (2.0 Å) with ARG10 (Figure 8A), the interaction of which was also discovered by Inserra and colleagues in experiments [29] in the solution NMR structure of the free solvated LsIA. Thus, our present simulation confirms that this CT-ARG10 salt bridge remains intact when LsIA is bound to $\alpha 7$ also.

In addition to this salt bridge interaction, our simulations identified a number of additional persistent hydrogen bonds which may further differentiate amidated from carboxylated LsIA. Another persistent hydrogen bond formed by amidated LsIA-CYS17 and the backbone carbonyl group of ASN15 in both types of LsIA bound to $\alpha 7$ was also observed in the present simulations (Figure 8). This intramolecular interaction is likely involved in drawing the C-terminus closer to loop 2 of α -helix of LsIAs (Figure 8A,B). Furthermore, the amidated LsIA-ASN15 also forms hydrogen bonds with the backbone of CYS17, with distances of 2.7 Å and 3.2 Å (Figure 8B). This additional hydrogen bonding pattern may play a role in the greater rigidity of CYS17 and ASN15 shown in the RMSF plots for amidated LsIA over its carboxylated analogue (Figure 2J). Finally, a persistent intramolecular hydrogen bond is also formed by ARG10 with the backbone of CYS4 (2.4 Å) in both amidated and carboxylated LsIAs, and may play a role in maintaining LsIA in its characteristic fold for both analogues.

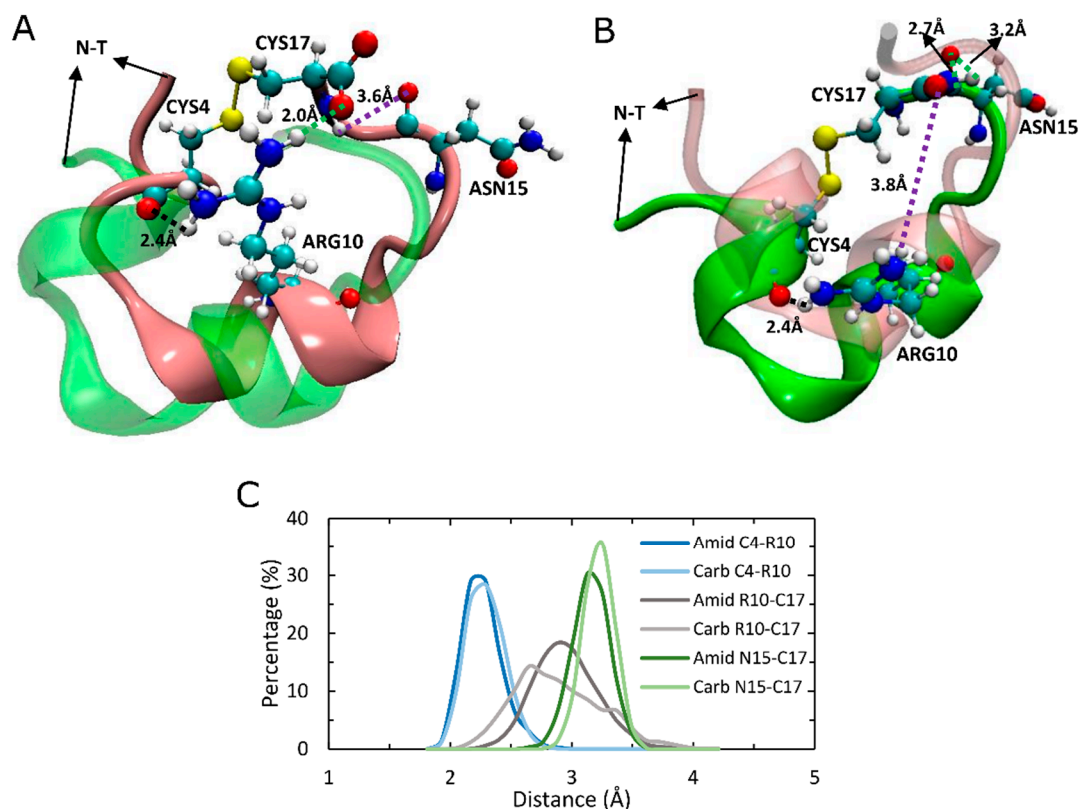


Figure 8. The intramolecular interactions within C-terminal carboxylated (mut) and amidated (wt) LsIAs by binding to human $\alpha 7$ nAChR. (A) The conformation of mut-LsIA (B) The conformation of wt-LsIA. The conformation of wt-LsIA in (A) and mut-LsIA in (B) is shown in transparent *green* and *pink* colors, respectively. (C) Distances (\AA) of intramolecular interactions between residues of wt-LsIA and mut-LsIA.

2.8. Changes in Inter-Subunit Contacts on the Five Interfaces of Adjacent $\alpha 7$ Subunits

The binding of amidated and carboxylated LsIAs to human $\alpha 7$ also elicits variations of contacts between residues at the interfaces between subunits of $\alpha 7$, which were examined using the Cytoscape [67] molecular analysis method. It is hereby proposed that structural disruptions to the integrity of inter-subunit contacts may have implications for the potency of conotoxins against nAChRs. Figure 9 shows the network representations of changes in inter-subunit contacts for the nodes (boxes) indicate interface residues, numbered and labeled by receptor chain (A–E). Each sub-figure shows residues at a different interface (e.g., Figure 9A shows the chain A–B interface, while Figure 9B shows the chain B–C interface). The edges (lines) connecting the nodes indicate possible contacts between the interface residues; red dot lines indicate contacts that are closer for the carboxylated form, green dash lines indicate contacts that are closer for the amidated form, while black lines indicate contacts that are similar for both forms. The nodes are color coded as follows: residues are colored red if they mainly have closer contacts with opposing interface residues at the *carboxylated* form, green if they mainly have closer contacts with opposing interface residues at the *amidated* form, and gray if their overall contacts with opposing residues are unchanged between the two forms.

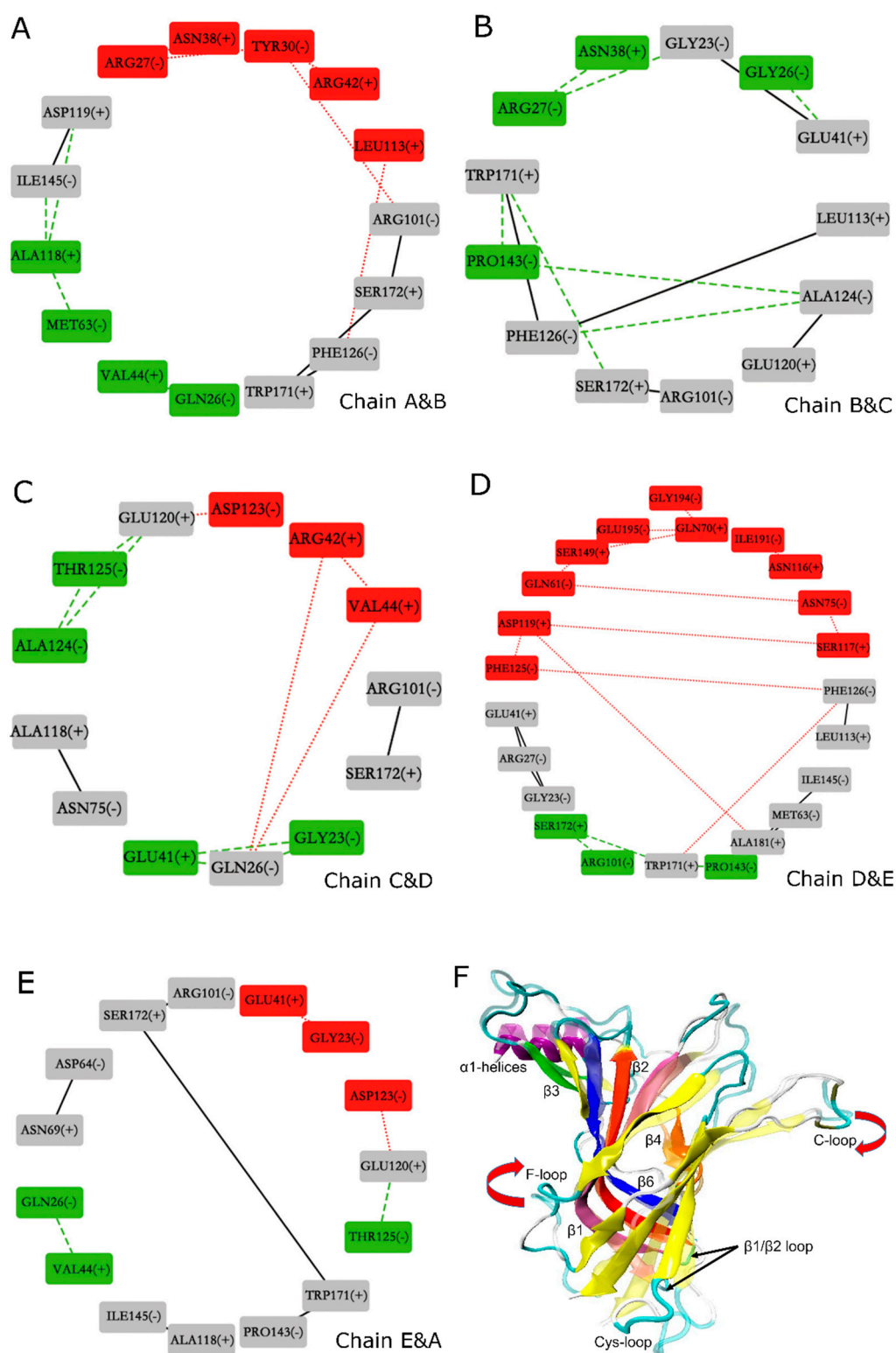


Figure 9. Comparison of differences in the interactions between principal (+) and complementary (-) interfaces of human α 7 nAChR after binding of amidated and carboxylated LsIAs. (A–E) Determination of interactive residues at five interfaces of α 7 nAChR via Cytoscape program. (F) Conformation of changes in the secondary structure of (+) face of LsIA bound receptors, where amidated LsIA bound face is shown in transparent color.

Overall, the predominance of grey nodes and edges shows that amidation generally caused similar inter-subunit contacts to C-T carboxylation. There is a slightly closer association between the interfaces for the amidated form, since all interfaces contain some residues that have closer association at the amidated form indicated by the presence of green nodes in all Figure 9A–E; but the interface between chains B and C does not have any residues that associate more closely at the carboxylated form, indicated by the absence of red nodes in Figure 9B. Nonetheless, certain interactions within interfaces of the carboxylated bound form which are weakened may have implications for LsIA binding to the LBD. On the other hand, interface contacts weakened by binding of amidated LsIA may also have implications for the inhibitory potency of this form of the toxin. Below, more details regarding which residues were involved in these disruptions in inter-subunit contacts, are discussed.

In general, acidic residues (ASP and GLU) at the inter-subunit interfaces have higher contacts with other residues for the amidated form. This can be demonstrated by considering certain residues situated in the N-terminal $\alpha 1$ helix(–) which interacted with the residues on loop between α -helix and $\beta 1$ (+), and resulted in pulling the N-terminal helices into a closer proximity in both amidated and carboxylated LsIA forms, and the gap between interfaces, therefore, was slightly shortened by toxin binding. For example, GLN26(–), were dominantly involved in interacting with both VAL44(+) (chains A&B and chains E&A) (Figure 9A,E) and with GLU41(+) (chains B&C and chains C&D) (Figure 9B,C), respectively. Interestingly, repulsive electrostatic interaction established by GLU120(+) and ASP123(–) (chains C&D and chains E&A) in carboxylated bound type, may elicit separation of the conjunctive interfaces (Figure 9C,E). In this case, residues on carboxylated LsIA probably lost contacts with the receptor due to the close proximity of several negative charges contributed by LsIA as well as the acidic residues of the two interfaces of the receptor. Additionally, on the boundary surface between chain D(+) and E(–) (Figure 9D), GLY194(–), GLU-195(–) and ILE-191(–) forms more interactions with GLN70(+) and ASN116(+) on $\beta 2$ and $\beta 4$ strands, respectively, in carboxylated bound form. These observed interactions may be related to a motion which may be described as an upward swing of the F-loop and a downward shift of the C-loop of chain E (Figure 9F), which has been suggested to promote agonist binding at apo chicken $\alpha 7$ -nAChR [15]. Furthermore, $\beta 6$ and C-loop have been determined as part of key determinants for binding of ACh to $\alpha 7$ nAChR [18].

Finally, another trend exhibited by examination of the network diagrams shows that several clusters of hydrophobic interactions form closer contacts with each other in the amidated form. Specifically, PRO143(–) on $\beta 6$ (–), forms hydrophobic interaction with TRP-171(+) (chains B&C and chains D&E) respectively on B-loop(+), shown in Figure 9B,D, which results in a longer distance between TRP-171(+) and S172(+) with PRO7 and ALA8 in amidated LsIA by triggering the shifting of B-loop(+) toward $\beta 6$ (–). Another unique hydrophobic interaction was determined between ALA118(+) and MET63(–) and ILE145(–) respectively, on chain A and B interface (Figure 9A). Among them, methionine residue is situated close to $\beta 1$ and $\beta 2$ loop, that were implicated in the conformational changes of the TMD of AChBP [68].

Taken together, the conclusions that can be drawn are that (1) binding of amidated LsIA favors inter-subunit interactions involving ASP and GLU near the agonist-binding site; and (2) binding of carboxylated LsIA favors a closer association between hydrophobic residues centered on PRO143(–) and ALA118(+), near the Cys-loop regions at the juxtamembrane domain. However, further studies are required for exploring the effects of the inter- $\alpha 7$ subunit contacts on stabilization and specificity of LsIA binding to the receptor.

3. Conclusions

In order to understand the importance of C-terminal of LsIA for selectively binding to human $\alpha 7$ nAChR at atomic level, we employed MD simulations to propose the determinants for the differential activity between naturally amidated and carboxylated LsIAs at the $\alpha 7$ nicotinic receptor. Simulations suggest that amidated LsIA-bound $\alpha 7$ exhibits higher fluctuations in loop C (at the canonical agonist binding site), as well as the juxtamembrane Cys-loop region. This variation in dynamic fluctuations

in both regions together may be related to differences in the capability of structural changes to be transmitted from the ECD down to the transmembrane domain when amidated, but not carboxylated, LsIA is bound to $\alpha 7$. Our findings also confirm a persistent intra-molecular salt bridge between ARG10 and the C-terminus in carboxylated LsIA is retained when bound to $\alpha 7$, and may be responsible for preventing the interactions between ARG10 and key residues in $\alpha 7$, such as ARG10 and TRP77(–) and LEU141(–), via cation- π and hydrogen bond interactions in amidated LsIA bound form, and therefore, affects the preferential selectivity of amidated LsIA to $\alpha 7$ nAChRs. This model is qualitatively consistent with the previous experimental findings which proposed a key role for ARG10 in forming interactions within the hydrophilic environment of the $\alpha 7$ binding pocket. Overall, carboxylation of the C-terminal reduces the selectivity of LsIA to $\alpha 7$ nAChR versus its native type.

Additionally, the impacts of binding of amidated and carboxylated LsIAs on the overall structure and inter-subunit contacts were examined using an inter-residue network analysis approach, suggesting a clockwise tilting of C and F loops upon binding to carboxylated LsIA, which is absent for amidated LsIA binding. The network analysis also indicates that proximate acidic residues ASP and GLU are possible at interfaces of $\alpha 7$ nAChR bound by the amidated LsIA, whereas the carboxylated counterpart disrupts these same-charge contacts while, instead, promoting closer contacts between interfacial hydrophobic residues. This approach may facilitate the determination of structural variations or changes in residue interactions at inter-subunit interfaces of the receptor upon binding of peptides.

Further exploration may be required for understanding specific impacts of residues of LsIA- $\alpha 7$ nAChR complexes on selectivity and stability of the ligands and the influence of inter-subunit contacts on native LsIA, via free binding energy calculation and experimental mutagenesis studies to probe the effects of the key residues, at both LsIA and $\alpha 7$, which are proposed in this present work. Furthermore, the carboxylation of C-terminals of conotoxins with known activity at receptors may need investigation in the future, such as studies on their binding potency and interactions with nAChRs or structural stability. The predicted molecular mechanism of LsIA binding to the neuronal nAChR, and in particular the possible roles of the C-terminal charge state, may facilitate a better understanding of the effect of C-terminal amidation/carboxylation on the binding potency of conotoxins at neuronal nAChRs, as most α -conotoxins and certain neuroactive peptides in other conotoxin subfamilies also possess a naturally amidated C-terminal in their structures. More broadly, these findings may assist in the design of novel peptides for nAChRs related disease and nAChR selective probes with high potency for understanding the structural and pharmacological features of nAChRs and other ion channels.

4. Methods

4.1. Homology Modeling

The sequence alignment of human $\alpha 7$ nAChR (UniProtKB:P36544) to *Ac-AChBP* was determined using multiple sequence alignment of human nAChR subunits $\alpha 4$ -10 and $\beta 2$ -4 with that of *Aplysia californica* acetylcholine binding protein (*Ac-AChBP*). Subsequently, homology models of amidated LsIA bound to the pentameric extracellular domain (ECD) of human $\alpha 7$ were generated using Modeler9v6 (Sali and Blundell, 1993) using the coordinates of *Ac-AChBP* co-crystallized with the double mutant α -conotoxin PnIA[A10L,D14K] (Protein Data Bank (PDB) accession code 2BR8) [6] as a template. One hundred models were generated, after which the model with the top DOPE [69] score was selected for simulations. The modification of the C-terminus of LsIA was conducted using Deep View (Swiss-PdbViewer, v4.1, Swiss Institute of Bioinformatics, Lausanne, Switzerland) [70] for changing the naturally amidated C-terminal to the carboxylated one.

4.2. Molecular Dynamics Simulations

The homology models of amidated and C-terminal carboxylated LsIAs anchored to human $\alpha 7$ nAChR, were centered in rectangular boxes with an initial size of $99.593 \times 99.593 \times 99.593 \text{ \AA}^3$ and $99.603 \times 99.603 \times 99.603 \text{ \AA}^3$, respectively, for fully submerging the $\alpha 7$ -LsIA complex structures in water.

Both of the systems were energy minimised using Gromacs 4 (v4.6.5, Science For Life Laboratory, Stockholm University and KTH, Stockholm, Sweden; and Biomedical Centre, Uppsala, Sweden) [71] with the CHARMM27 forcefield and were solvated with water by TIP3P water model [72]. Na⁺ and Cl⁻ ions were added for achieving a concentration of 0.15 M and neutralizing the charged amino acid residues in the two systems. For LsIA- α 7 complex, 80 Na⁺ and 70 Cl⁻ were added, whereas 85 Na⁺ and 70 Cl⁻ were introduced in the carboxylated LsIA bound complex. Both systems were energy minimized for up to 1000 time steps utilizing the steepest descent minimisation algorithm. The temperature was regulated by the velocity-rescale method [73,74], increasing from 0 K to 300 K over 100 ps in NPT ensembles with pressure under 1 atm. In order to restrain all protein molecules in the systems, the LINCS algorithm [75] was implemented with a time step of 2 fs. The cutoff of van der Waals interaction was set to 12 Å with a smooth switch of 10 Å, meanwhile, the electrostatic energy was calculated via Particle Mesh Ewald (PME) method [76]. Subsequently, the production runs under constant NPT conditions were conducted for at least 30 ns with restraints removed. Production simulations of both amidated and carboxylated LsIA- α 7 complexes were performed using different random seeds to set random initial particle velocities, with 12 independent simulations for each system. Since α 7 nAChR contains five equivalent interfaces, the total amount of trajectory collected for analysis of α 7(+) α 7(-) interfaces were at least 3.6 microseconds (2 systems \times 12 independent simulations \times 30 ns \times 5 interfaces). Analyses were performed either on data obtained as an average over the independent simulation trajectories, or over independent trajectories as well as interfaces, as noted in the Results and Discussion. In this study, the frames were saved every 10 ps for analyses for all trajectories.

4.3. Structural Visualization and Analysis

Conformations of the LsIA- α 7 complexes obtained by MD simulations, were identified and analysed using a number of computational methods. Visual Molecular Dynamics (VMD) [77] was used for observing MD simulation results and production of figures of binding conformations. Root-mean-square deviation (RMSD) and RMS fluctuation (RMSF) were calculated using the GROMACS suite of analysis tools; and were used for evaluation of structure stability, flexibility and rigidity of the protein complexes. The average structures generated from the *rmsf* command implemented in GROMACS were examined using Cytoscape [67], which is a program for visualization and comparison of inter-residue interaction networks in protein complexes. The *mindist* command implemented in GROMACS was used for determining numbers and distances of contacts between interactive residues of ligand and receptor with a cutoff of 4.5 Å. In all Results and Discussion sections, the five subunits of α 7 nAChR are labeled chains A to E, while the five amidated or carboxylated LsIA conotoxins binding at the interfaces between the α 7(+) α 7(-) subunits are labeled chains F to J.

RMSD, RMSF and *gmx_mindist* analysis are based upon different manipulations of MD simulation trajectories. RMSD of each subunit/ligand was the average based on 12 seeds of MD simulation trajectories with each seed running for around 40 ns with the segment beyond 30 ns cut off. Therefore, the total amount of time shown in Figure 2A–D is 30 ns. The RMSF of each subunit/ligand was calculated based upon the original MD simulation data. 7a and 7c are short for amidated LsIA and carboxylated LsIA bound form, respectively. The *Gmx_mindist* of each paired residue was calculated based upon the whole trajectory, with the first 10 ns of each individual seed being cut off.

Author Contributions: Conceptualization, J.W. and A.H.; methodology, J.W. and A.H.; writing—original draft preparation, J.W.; writing—review and editing J.W. and A.H., supervision, A.H.; funding acquisition, A.H.

Funding: A.H. and J.W. are grateful for the provision of computational resources by the National Computational Infrastructure (NCI) and the Pawsey Supercomputing Centre, Australia, which are funded by the Australian Government. This work is supported by The Australian Research Council Discovery Project grant DP150103990.

Acknowledgments: A.H. and J.W. thank David J. Adams (University of Wollongong, Australia) for helpful discussions.

Conflicts of Interest: The authors declare no conflict of interest.

References

1. Lebbe, E.K.M.; Peigneur, S.; Maiti, M.; Devi, P.; Ravichandran, S.; Lescrinier, E.; Ulens, C.; Waelkens, E.; D'Souza, L.; Herdewijn, P.; et al. Structure-Function Elucidation of a New α -Conotoxin, Lo1a, from *Conus longurionis*. *J. Biol. Chem.* **2014**, *289*, 9573–9583. [[CrossRef](#)] [[PubMed](#)]
2. Song, C.; Corry, B. Role of acetylcholine receptor domains in ion selectivity. *Biochim. Biophys. Acta (Bba) Biomembr.* **2009**, *1788*, 1466–1473. [[CrossRef](#)] [[PubMed](#)]
3. Hurst, R.; Rollema, H.; Bertrand, D. Nicotinic acetylcholine receptors: From basic science to therapeutics. *Pharmacol. Ther.* **2013**, *137*, 22–54. [[CrossRef](#)]
4. Hogg, R.C.; Hopping, G.; Alewood, P.F.; Adams, D.J.; Bertrand, D. α -Conotoxins PnIA and [A10L]PnIA Stabilize Different States of the α 7-L247T Nicotinic Acetylcholine Receptor. *J. Biol. Chem.* **2003**, *278*, 26908–26914. [[CrossRef](#)] [[PubMed](#)]
5. Pohanka, M. Alpha7 Nicotinic Acetylcholine Receptor Is a Target in Pharmacology and Toxicology. *Int. J. Mol. Sci.* **2012**, *13*, 2219–2238. [[CrossRef](#)]
6. Celie, P.H.N.; Kasheverov, I.E.; Mordvintsev, D.Y.; Hogg, R.C.; van Nierop, P.; van Elk, R. Crystal structure of nicotinic acetylcholine receptor homolog AChBP in complex with an alpha-conotoxin PnIA variant. *Nat. Struct. Mol. Biol.* **2005**, *12*, 582–588. [[CrossRef](#)] [[PubMed](#)]
7. Kalkman, H.O.; Feuerbach, D. Modulatory effects of α 7 nAChRs on the immune system and its relevance for CNS disorders. *Cell. Mol. Life Sci.* **2016**, *73*, 2511–2530. [[CrossRef](#)]
8. D'Andrea, M.R.; Nagele, R.G. Targeting the Alpha 7 Nicotinic Acetylcholine Receptor to Reduce Amyloid Accumulation in Alzheimer's Disease Pyramidal Neurons. *Curr. Pharm. Des.* **2006**, *12*, 677–684. [[CrossRef](#)]
9. Taly, A.; Corringier, P.-J.; Guedin, D.; Lestage, P.; Changeux, J.-P. Nicotinic receptors: Allosteric transitions and therapeutic targets in the nervous system. *Nat. Rev. Drug Discov.* **2009**, *8*, 733–750. [[CrossRef](#)] [[PubMed](#)]
10. Söderman, A.; Mikkelsen, J.D.; West, M.J.; Christensen, D.Z.; Jensen, M.S. Activation of nicotinic α 7 acetylcholine receptor enhances long term potentiation in wild type mice but not in APPswe/PS1 Δ E9 mice. *Neurosci. Lett.* **2011**, *487*, 325–329. [[CrossRef](#)]
11. Ulens, C.; Hogg, R.C.; Celie, P.H.; Bertrand, D.; Tsetlin, V.; Smit, A.B.; Sixma, T.K. Structural determinants of selective α -conotoxin binding to a nicotinic acetylcholine receptor homolog AChBP. *Proc. Natl. Acad. Sci. USA* **2006**, *103*, 3615–3620. [[CrossRef](#)] [[PubMed](#)]
12. Bourne, Y.; Talley, T.T.; Hansen, S.B.; Palmer, T.; Marchot, P. Crystal structure of a Cbtx-AChBP complex reveals essential interactions between snake [alpha]-neurotoxins and nicotinic receptors. *EMBO J.* **2005**, *24*, 1512–1522. [[CrossRef](#)] [[PubMed](#)]
13. Brejc, K.; van Dijk, W.J.; Klaassen, R.V.; Schuurmans, M.; Oost, J.V.D.; Smit, A.B.; Sixma, T.K. Crystal structure of an ACh-binding protein reveals the ligand-binding domain of nicotinic receptors. *Nature* **2001**, *411*, 269–276. [[CrossRef](#)]
14. Yi, M.; Tjong, H.; Zhou, H.-X. Spontaneous conformational change and toxin binding in α 7 acetylcholine receptor: Insight into channel activation and inhibition. *Proc. Natl. Acad. Sci. USA* **2008**, *105*, 8280–8285. [[CrossRef](#)]
15. Maricq, A.V.; Peterson, A.S.; Brake, A.J.; Myers, R.M.; Julius, D. Primary structure and functional expression of the 5HT3 receptor, a serotonin-gated ion channel. *Science* **1991**, *254*, 432–437. [[CrossRef](#)] [[PubMed](#)]
16. Harel, M.; Kashner, R.; Nicolas, A.; Guss, J.M.; Balass, M.; Fridkin, M.; Smit, A.B.; Brejc, K.; Sixma, T.K.; Katchalski-Katzir, E.; et al. The Binding Site of Acetylcholine Receptor as Visualized in the X-ray Structure of a Complex between α -Bungarotoxin and a Mimotope Peptide. *Neuron* **2001**, *32*, 265–275. [[CrossRef](#)]
17. Dutertre, S.; Nicke, A.; Tyndall, J.D.A.; Lewis, R.J. Determination of α -conotoxin binding modes on neuronal nicotinic acetylcholine receptors. *J. Mol. Recognit.* **2004**, *17*, 339–347. [[CrossRef](#)] [[PubMed](#)]
18. Yu, R.; Craik, D.J.; Kaas, Q. Blockade of neuronal α 7-nAChR by α -conotoxin ImI explained by computational scanning and energy calculations. *PLoS Comput. Biol.* **2011**, *7*, e1002011. [[CrossRef](#)]
19. Hansen, S.B.; Talley, T.T.; Radić, Z.; Taylor, P. Structural and Ligand Recognition Characteristics of an Acetylcholine-binding Protein from *Aplysia californica*. *J. Biol. Chem.* **2004**, *279*, 24197–24202. [[CrossRef](#)]
20. Azam, L.; McIntosh, J.M. Alpha-conotoxins as pharmacological probes of nicotinic acetylcholine receptors. *Acta Pharmacol. Sin.* **2009**, *30*, 771–783. [[CrossRef](#)]
21. Kasheverov, I.E.; Zhmak, M.N.; Khrushov, A.Y.; Tsetlin, V.I. Design of New α -Conotoxins: From Computer Modeling to Synthesis of Potent Cholinergic Compounds. *Mar. Drugs* **2011**, *9*. [[CrossRef](#)] [[PubMed](#)]

22. Olivera, B.M.; Rivier, J.; Clark, C.; Ramilo, C.A.; Corpuz, G.P.; Abogadie, F.C.; Mena, E.E.; Woodward, S.R.; Hillyard, D.R.; Cruz, L.J. Diversity of Conus neuropeptides. *Science* **1990**, *249*, 257–263. [[CrossRef](#)]
23. Quiram, P.A.; McIntosh, J.M.; Sine, S.M. Pairwise Interactions between Neuronal $\alpha 7$ Acetylcholine Receptors and α -Conotoxin PnIB. *J. Biol. Chem.* **2000**, *275*, 4889–4896. [[CrossRef](#)]
24. Hoggard, M.F.; Rodriguez, A.M.; Cano, H.; Clark, E.; Tae, H.-S.; Adams, D.J.; Godenschwege, T.A.; Marí, F. In vivo and in vitro testing of native α -conotoxins from the injected venom of *Conus purpurascens*. *Neuropharmacology* **2017**, *127*, 253–259. [[CrossRef](#)] [[PubMed](#)]
25. McIntosh, J.M.; Santos, A.D.; Olivera, B.M. Conus peptides targeted to specific nicotinic acetylcholine receptor subtypes. *Annu. Rev. Biochem.* **1999**, *68*, 59–88. [[CrossRef](#)] [[PubMed](#)]
26. Suresh, A.; Hung, A. Molecular simulation study of the unbinding of α -conotoxin [Y4E]GID at the $\alpha 7$ and $\alpha 4\beta 2$ neuronal nicotinic acetylcholine receptors. *J. Mol. Graph. Model.* **2016**, *70*, 109–121. [[CrossRef](#)]
27. Armishaw, C.J. Synthetic α -conotoxin mutants as probes for studying nicotinic acetylcholine receptors and in the development of novel drug leads. *Toxins* **2010**, *2*, 1471–1499. [[CrossRef](#)]
28. Abraham, N.; Healy, M.; Ragnarsson, L.; Brust, A.; Alewood, P.F.; Lewis, R.J. Structural mechanisms for [alpha]-conotoxin activity at the human [alpha]3[beta]4 nicotinic acetylcholine receptor. *Sci. Rep.* **2017**, *7*, 45466. [[CrossRef](#)]
29. Inserra, M.C.; Kompella, S.N.; Vetter, I.; Brust, A.; Daly, N.L.; Cuny, H.; Craik, D.J.; Alewood, P.F.; Adams, D.J.; Lewis, R.J. Isolation and characterization of α -conotoxin LsIA with potent activity at nicotinic acetylcholine receptors. *Biochem. Pharmacol.* **2013**, *86*, 791–799. [[CrossRef](#)]
30. Chi, S.-W.; Kim, D.-H.; Olivera, B.M.; McIntosh, J.M.; Han, K.-H. Solution conformation of alpha-conotoxin GIC, a novel potent antagonist of alpha3beta2 nicotinic acetylcholine receptors. *Biochem. J.* **2004**, *380*, 347–352. [[CrossRef](#)]
31. Dutertre, S.; Lewis, R.J. Toxin insights into nicotinic acetylcholine receptors. *Biochem. Pharmacol.* **2006**, *72*, 661–670. [[CrossRef](#)] [[PubMed](#)]
32. Nicke, A.; Loughnan, M.L.; Millard, E.L.; Alewood, P.F.; Adams, D.J.; Daly, N.L.; Craik, D.J.; Lewis, R.J. Isolation, Structure, and Activity of GID, a Novel $\alpha 4/7$ -Conotoxin with an Extended N-terminal Sequence. *J. Biol. Chem.* **2003**, *278*, 3137–3144. [[CrossRef](#)]
33. Quiram, P.A.; Sine, S.M. Structural Elements in α -Conotoxin Iml Essential for Binding to Neuronal $\alpha 7$ Receptors. *J. Biol. Chem.* **1998**, *273*, 11007–11011. [[CrossRef](#)] [[PubMed](#)]
34. Wakamatsu, K.; Kohda, D.; Hatanaka, H.; Lancelin, J.M.; Ishida, Y.; Oya, M.; Nakamura, H.; Inagaki, F.; Sato, K. Structure-activity relationships of μ -conotoxin GIIIA: Structure determination of active and inactive sodium channel blocker peptides by NMR and simulated annealing calculations. *Biochemistry* **1992**, *31*, 12577–12584. [[CrossRef](#)] [[PubMed](#)]
35. Zhang, M.-M.; Green, B.R.; Catlin, P.; Fiedler, B.; Azam, L.; Chadwick, A.; Terlau, H.; McArthur, J.R.; French, R.J.; Gulyas, J.; et al. Structure/Function Characterization of μ -Conotoxin KIIIA, an Analgesic, Nearly Irreversible Blocker of Mammalian Neuronal Sodium Channels. *J. Biol. Chem.* **2007**, *282*, 30699–30706. [[CrossRef](#)] [[PubMed](#)]
36. Adams, D.J.; Smith, A.B.; Schroeder, C.I.; Yasuda, T.; Lewis, R.J. ω -Conotoxin CVID Inhibits a Pharmacologically Distinct Voltage-sensitive Calcium Channel Associated with Transmitter Release from Preganglionic Nerve Terminals. *J. Biol. Chem.* **2003**, *278*, 4057–4062. [[CrossRef](#)] [[PubMed](#)]
37. Kohno, T.; Kim, J.I.; Kobayashi, K.; Koder, Y.; Maeda, T.; Sato, K. Three-Dimensional Structure in Solution of the Calcium Channel Blocker. omega-Conotoxin MVIIA. *Biochemistry* **1995**, *34*, 10256–10265. [[CrossRef](#)]
38. Rajendra, W.; Armugam, A.; Jeyaseelan, K. Toxins in anti-nociception and anti-inflammation. *Toxicon* **2004**, *44*, 1–17. [[CrossRef](#)]
39. Livett, B.G.; Sandall, D.W.; Keays, D.; Down, J.; Gayler, K.R.; Satkunanathan, N.; Khalil, Z. Therapeutic applications of conotoxins that target the neuronal nicotinic acetylcholine receptor. *Toxicon* **2006**, *48*, 810–829. [[CrossRef](#)]
40. Satkunanathan, N.; Livett, B.; Gayler, K.; Sandall, D.; Down, J.; Khalil, Z. Alpha-conotoxin Vc1.1 alleviates neuropathic pain and accelerates functional recovery of injured neurones. *Brain Res.* **2005**, *1059*, 149–158. [[CrossRef](#)]
41. Gao, B.; Peng, C.; Yang, J.; Yi, Y.; Zhang, J.; Shi, Q. Cone Snails: A Big Store of Conotoxins for Novel Drug Discovery. *Toxins* **2017**, *9*, 397. [[CrossRef](#)] [[PubMed](#)]

42. Wu, C.-H.; Lee, C.-H.; Ho, Y.-S. Nicotinic Acetylcholine Receptor-Based Blockade: Applications of Molecular Targets for Cancer Therapy. *Clin. Cancer Res.* **2011**, *17*, 3533–3541. [[CrossRef](#)] [[PubMed](#)]
43. Quiram, P.A.; Jones, J.J.; Sine, S.M. Pairwise Interactions between Neuronal $\alpha 7$ Acetylcholine Receptors and α -Conotoxin ImI. *J. Biol. Chem.* **1999**, *274*, 19517–19524. [[CrossRef](#)]
44. Eddins, D.; Sproul, A.D.; Lyford, L.K.; McLaughlin, J.T.; Rosenberg, R.L. Glutamate 172, essential for modulation of L247T $\alpha 7$ ACh receptors by Ca^{2+} , lines the extracellular vestibule. *Am. J. Physiol. Cell Physiol.* **2002**, *283*, C1454–C1460. [[CrossRef](#)]
45. Kasheverov, I.E.; Chugunov, A.O.; Kudryavtsev, D.S.; Ivanov, I.A.; Zhmak, M.N.; Shelukhina, I.V.; Spirova, E.N.; Tabakmakher, V.M.; Zelepuga, E.A.; Efremov, R.G.; et al. High-Affinity α -Conotoxin PnIA Analogs Designed on the Basis of the Protein Surface Topography Method. *Sci. Rep.* **2016**, *6*, 36848. Available online: <https://www.nature.com/articles/srep36848#supplementary-information> (accessed on 11 October 2018). [[CrossRef](#)]
46. Barrantes, F.J. *The Nicotinic Acetylcholine Receptor Current Views and Future Trends*; Springer: Berlin/Heidelberg, Germany, 1998.
47. Lebbe, E.K.M.; Peigneur, S.; Wijesekara, I.; Tytgat, J. Conotoxins targeting nicotinic acetylcholine receptors: An overview. *Mar. Drugs* **2014**, *12*, 2970–3004. [[CrossRef](#)] [[PubMed](#)]
48. Boffi, J.C.; Marcovich, I.; Gill-Thind, J.K.; Corradi, J.; Collins, T.; Lipovsek, M.M.; Moglie, M.; Plazas, P.V.; Craig, P.O.; Millar, N.S.; et al. Differential Contribution of Subunit Interfaces to $\alpha 9\alpha 10$ Nicotinic Acetylcholine Receptor Function. *Mol. Pharmacol.* **2017**, *91*, 250–262. [[CrossRef](#)] [[PubMed](#)]
49. Lester, H.A.; Dibas, M.I.; Dahan, D.S.; Leite, J.F.; Dougherty, D.A. Cys-loop receptors: New twists and turns. *Trends Neurosci.* **2004**, *27*, 329–336. [[CrossRef](#)] [[PubMed](#)]
50. Tsigelny, I.; Sugiyama, N.; Sine, S.M.; Taylor, P. A model of the nicotinic receptor extracellular domain based on sequence identity and residue location. *Biophys. J.* **1997**, *73*, 52–66. [[CrossRef](#)]
51. Dutertre, S.; Ulens, C.; Büttner, R.; Fish, A.; van Elk, R.; Kendel, Y.; Hopping, G.; Alewood, P.F.; Schroeder, C.; Nicke, A.; et al. AChBP-targeted α -conotoxin correlates distinct binding orientations with nAChR subtype selectivity. *EMBO J.* **2007**, *26*, 3858–3867. [[CrossRef](#)]
52. Sahu, B.S.; Obbineni, J.M.; Sahu, G.; Singh, P.K.; Sonawane, P.J.; Sasi, B.K.; Allu, P.K.R.; Maji, S.K.; Bera, A.K.; Senapati, S.; et al. Molecular interactions of the physiological anti-hypertensive peptide catestatin with the neuronal nicotinic acetylcholine receptor. *J. Cell Sci.* **2012**, *125*, 2323–2337. [[CrossRef](#)]
53. Peng, W.; Ding, F. Biomolecular recognition of antagonists by $\alpha 7$ nicotinic acetylcholine receptor: Antagonistic mechanism and structure–activity relationships studies. *Eur. J. Pharm. Sci.* **2015**, *76*, 119–132. [[CrossRef](#)]
54. Hilf, R.J.C.; Dutzler, R. Structure of a potentially open state of a proton-activated pentameric ligand-gated ion channel. *Nature* **2009**, *457*, 115–118. [[CrossRef](#)]
55. Lee, W.Y.; Sine, S.M. Principal pathway coupling agonist binding to channel gating in nicotinic receptors. *Nature* **2005**, *438*, 243–247. [[CrossRef](#)] [[PubMed](#)]
56. Unwin, N.; Fujiyoshi, Y. Gating movement of acetylcholine receptor caught by plunge-freezing. *J. Mol. Biol.* **2012**, *422*, 617–634. [[CrossRef](#)]
57. Hibbs, R.E.; Gouaux, E. Principles of activation and permeation in an anion-selective Cys-loop receptor. *Nature* **2011**, *474*, 54. Available online: <https://www.nature.com/articles/nature10139#supplementary-information> (accessed on 15 January 2019). [[CrossRef](#)]
58. Lummis, S.C.R.; Beene, D.L.; Lee, L.W.; Lester, H.A.; Broadhurst, R.W.; Dougherty, D.A. Cis-trans isomerization at a proline opens the pore of a neurotransmitter-gated ion channel. *Nature* **2005**, *438*, 248–252. [[CrossRef](#)] [[PubMed](#)]
59. Baenziger, J.E.; Hénault, C.M.; Therien, J.P.D.; Sun, J. Nicotinic acetylcholine receptor–lipid interactions: Mechanistic insight and biological function. *Biochim. Biophys. Acta (BBA) Biomembr.* **2015**, *1848*, 1806–1817. [[CrossRef](#)]
60. Noridomi, K.; Watanabe, G.; Hansen, M.N.; Han, G.W.; Chen, L. Structural insights into the molecular mechanisms of myasthenia gravis and their therapeutic implications. *eLife* **2017**, *6*, e23043. [[CrossRef](#)]
61. Armishaw, C.; Jensen, A.A.; Balle, T.; Clark, R.J.; Harpsøe, K.; Skonberg, C.; Liljefors, T.; Strømgaard, K. Rational Design of α -Conotoxin Analogues Targeting $\alpha 7$ Nicotinic Acetylcholine Receptors: Improved antagonistic activity by incorporation of proline derivatives. *J. Biol. Chem.* **2009**, *284*, 9498–9512. [[CrossRef](#)]
62. Gallivan, J.P.; Dougherty, D.A. Cation- π interactions in structural biology. *Proc. Natl. Acad. Sci. USA* **1999**, *96*, 9459–9464. [[CrossRef](#)] [[PubMed](#)]

63. Grishin, A.A.; Cuny, H.; Hung, A.; Clark, R.J.; Brust, A.; Akondi, K.; Alewood, P.F.; Craik, D.J.; Adams, D.J. Identifying Key Amino Acid Residues That Affect α -Conotoxin A α B Inhibition of α 3 β 4 Nicotinic Acetylcholine Receptors. *J. Biol. Chem.* **2013**, *288*, 34428–34442. [[CrossRef](#)]
64. Ellison, M.; Gao, F.; Wang, H.-L.; Sine, S.M.; McIntosh, J.M.; Olivera, B.M. α -Conotoxins ImI and ImII Target Distinct Regions of the Human α 7 Nicotinic Acetylcholine Receptor and Distinguish Human Nicotinic Receptor Subtypes. *Biochemistry* **2004**, *43*, 16019–16026. [[CrossRef](#)]
65. Gay, E.A.; Giniatullin, R.; Skorinkin, A.; Yakel, J.L. Aromatic residues at position 55 of rat α 7 nicotinic acetylcholine receptors are critical for maintaining rapid desensitization. *J. Physiol.* **2008**, *586*, 1105–1115. [[CrossRef](#)]
66. Kang, T.S.; Vivekanandan, S.; Jois, S.D.S.; Kini, R.M. Effect of C-Terminal Amidation on Folding and Disulfide-Pairing of α -Conotoxin ImI. *Angew. Chem. Int. Ed.* **2005**, *44*, 6333–6337. [[CrossRef](#)] [[PubMed](#)]
67. Shannon, P.; Markiel, A.; Ozier, O.; Baliga, N.S.; Wang, J.T.; Ramage, D.; Amin, N.; Schwikowski, B.; Ideker, T. Cytoscape: A software environment for integrated models of biomolecular interaction networks. *Genome Res.* **2003**, *13*, 2498–2504. [[CrossRef](#)]
68. Gao, F.; Bren, N.; Burghardt, T.P.; Hansen, S.; Henchman, R.H.; Taylor, P.; McCammon, J.A.; Sine, S.M. Agonist-mediated Conformational Changes in Acetylcholine-binding Protein Revealed by Simulation and Intrinsic Tryptophan Fluorescence. *J. Biol. Chem.* **2005**, *280*, 8443–8451. [[CrossRef](#)]
69. Shen, M.-Y.; Sali, A. Statistical potential for assessment and prediction of protein structures. *Protein Sci. A Publ. Protein Soc.* **2006**, *15*, 2507–2524. [[CrossRef](#)] [[PubMed](#)]
70. Guex, N.; Peitsch, M.C. SWISS-MODEL and the Swiss-Pdb Viewer: An environment for comparative protein modeling. *Electrophoresis* **1997**, *18*, 2714–2723. [[CrossRef](#)] [[PubMed](#)]
71. Hess, B.; Kutzner, C.; van der Spoel, D.; Lindahl, E. GROMACS 4: Algorithms for Highly Efficient, Load-Balanced, and Scalable Molecular Simulation. *J. Chem. Theory Comput.* **2008**, *4*, 435–447. [[CrossRef](#)]
72. Mark, P.; Nilsson, L. Structure and Dynamics of the TIP3P, SPC, and SPC/E Water Models at 298 K. *J. Phys. Chem. A* **2001**, *105*, 9954–9960. [[CrossRef](#)]
73. Quigley, D.; Probert, M.I.J. Langevin dynamics in constant pressure extended systems. *J. Chem. Phys.* **2004**, *120*, 11432–11441. [[CrossRef](#)] [[PubMed](#)]
74. Bussi, G.; Donadio, D.; Parrinello, M. Canonical sampling through velocity rescaling. *J. Chem. Phys.* **2007**, *126*, 014101. [[CrossRef](#)] [[PubMed](#)]
75. Hess, B.; Bekker, H.; Berendsen, H.J.C.; Fraaije, J.G.E.M. LINCS: A linear constraint solver for molecular simulations. *J. Comput. Chem.* **1997**, *18*, 1463–1472. [[CrossRef](#)]
76. Essmann, U.; Perera, L.; Berkowitz, M.L.; Darden, T.; Lee, H.; Pedersen, L.G. A smooth particle mesh Ewald method. *J. Chem. Phys.* **1995**, *103*, 8577–8593. [[CrossRef](#)]
77. Humphrey, W.; Dalke, A.; Schulten, K. VMD: Visual molecular dynamics. *J. Mol. Graph.* **1996**, *14*, 33–38. [[CrossRef](#)]

